Journal of Ocean Engineering and Marine Energy (2023) 9:495–513
https://doi.org/10.1007/s40722-023-00280-3

RESEARCH ARTICLE

# Modelling 3D dynamics of offshore lattice jib cranes by means of the rigid finite element method

Adamiec-Wójcik Iwona[1] · Brzozowska Lucyna[1] · Drąg Łukasz[1] · Metelski Marek[2] · Wojciech Stanisław[1]

Received: 7 July 2022 / Accepted: 8 March 2023 / Published online: 4 May 2023


**Abstract**
Offshore cranes require particularly careful design due to the difficult environmental conditions in which they work. This paper presents a 3D model of the dynamics of an offshore crane with a truss jib formulated by means of the rigid finite element method. The inertial features of the truss members are assigned to nodes whose rotational and translational displacements are degrees of freedom. Flexible features of the truss members are modelled by massless and dimensionless spring–damping elements (sde). The computer programme developed on the basis of the model is verified and validated, and good correspondence of the authors' own results with those obtained using commercial FEM package is achieved. Computer simulations are carried out for the light crane used on the wind platforms. The influence of the base movements (sea waves) on the system are also investigated. Lifting a load from a supply vessel and the load on the system during rotational movement of the crane are simulated too. Finally, conclusions concerning the influence of the movement conditions on the overload coefficient and deflections of the crane boom are formulated.

**Keywords** Offshore lattice crane · Rigid finite element method · Truss structure · Sea wave motion · Overload

## 1 Introduction

Offshore cranes analysed in this paper operate in difficult environmental conditions. They ensure transportation to/from vessels as well as wind and tidal platforms. Sea waves, sea currents and wind considerably influence the work of these cranes. Thus, both for the safety and cost reasons, these types of cranes are often designed with lattice jibs, the important feature of which is the relatively high strength and low weight.

For numerical simulations, designers usually use either commercial software (ROBOT, Abaqus, FemUp) based on the Finite Element Method (FEM) or dedicated software developed for the needs of a specific company. In the latter case, it is possible to develop an interface adapted to the needs of the user (designers, computing specialists). It is therefore also possible to develop special programmes for the simulations and optimisation of drives and Automatic Overload Protection Systems (AOPS).

Models used in both commercial and dedicated packages are often presented in the literature, especially in connection with the problems of drive control. Reviews of existing models and especially control strategies are presented by Abdel-Rahman et al. (2003), Ramli et al. (2017) and also by Cao and Li (2020). In some research, the flexibility of the boom, the rope system or the motion of the base (ship or platform) caused by sea waves and sea currents is omitted. In these cases, the models and the range of dynamic analysis do not differ from those carried out for stationary cranes.

In the last few decades, the number of papers devoted to modelling of stationary and offshore cranes has grown rapidly. Thus, here, we refer mainly to those dealing with offshore cranes, while rarely mentioning others. Abdel-Rahman et al. (2003) identify two approaches to modelling cranes: distributed mass and lumped-mass models. However, flexible booms are also modelled by means of the finite element method (FEM) (Ren et al. 2008; Trąbka 2016; Maourane and Szabó 2020) or so-called multibody approach (Cha et al. 2010; Cibicik and Egeland 2019) including the segment method (Bak and Hansen 2013; Rong et al. 2019) and the

✉ Adamiec-Wójcik Iwona
i.adamiec@ath.bielsko.pl

[1] University of Bielsko-Biala, Willowa 2, 43-309 Bielsko-Biała, Poland

[2] Protea S.A., Galaktyczna 30A, 80-299 Gdańsk, Poland

rigid finite element method (RFEM) (Wittbrodt et al. 2013). Different types of cranes such as container cranes (Hong and Ngo 2012; Arena et al. 2015; Raja Ismail et al. 2015), jib cranes (Osiński and Wojciech 1998; Doçi et al. 2016) and knuckle-boom cranes (Bak and Hansen 2013; Chu et al. 2015, 2018; Adamiec-Wójcik et al. 2019; Cibicik and Egeland 2019) are analysed.

The rigid finite element method has been used successfully for modelling different types of cranes mounted on platforms or vessels subject to wave motion (Osiński and Wojciech 1998; Osiński et al. 2004; Wittbrodt et al. 2013). Osiński and Wojciech (1998) and Osiński et al. (2004) deal with planar dynamic analysis of a crane. Critical phases of handling operations of a load while a supply ship is moving are considered. Modelling emergency conditions requires taking into account the flexibility of the boom. Osiński et al. (2004) use the planar model to select drive functions of a hoisting winch to minimise rope overload and analyse required velocities, while the load is lifted. Selection of drive functions of the hoisting winch during lifting operations is discussed by Maczyński and Wojciech (2011). Sea waves are described using harmonic functions. Some other examples of applications of RFEM to modelling dynamics of offshore devices during handling operations can be found in Urbaś et al. (2010), Krukowski and Maczyński (2013), Wittbrodt et al. (2013) and Adamiec-Wójcik et al. (2018). A gantry crane used for transporting a Blowout Preventor (BOP), while subject to sea waves, is discussed by Urbaś et al. (2010). Krukowski and Maczyński (2013) analyse dynamics of an offshore pedestal crane with three flexible components (pedestal, frame and boom). All three components are modelled using the rigid finite element method, although in each case, it is a slightly different approach; elements with variable length are used for the pedestal model.

The RFEM used for discretisation of lattice booms was only applied to solve static problems or in analysis of linear vibrations. This paper is an extension of the application of the RFEM to dynamics of cranes with lattice jibs. The advantage of the RFEM in relation to classical methods such as the finite element methods is the ease of taking into account additional concentrated masses and rigid mass elements. Static problems of lattice booms were discussed by Nowak et al. (2017). The model of the crane dynamics presented in this paper takes into account motion of the base on which the crane is mounted (platform or vessel), as well as bending, torsional, longitudinal flexibilities and shear of the boom truss members. The flexibility both of the rope system of the load lifting mechanism and of the luffing system are also considered. The model and the computer programme are validated by comparing the authors' own results with those obtained using the ROBOT commercial software package. The numerical effectiveness of the crane dynamics model is evaluated together with its applications in modelling dynamics of a service crane used on wind platforms for typical transport tasks such as lifting a load and rotation of the column. The numerical calculations carried out make it possible to assess the impact of the work performed, with variable boom inclination and different load lifting speeds, on the boom deflections and overloading in the rope system.

## 2 Model of the crane

Figure 1a shows one of the lattice boom cranes intended for servicing wind farms, manufactured by Protea, while the model of the crane is shown in Fig. 1b.

The following notation of the coordinate systems is introduced:

{}—global (inertial) system assigned to the sea bottom.

$\{\}\hat{}$—system assigned to the moving base of the crane (vessel or platform).

$\{\}^{-}$—system assigned to the rotary part of the crane.

$\{\}'$—system assigned to the boom.

$\{\}_{\hat{\mathrm{L}}}$—system assigned to the deck of the cargo unit.

$\alpha = \psi_J$—boom inclination angle.

To describe the orientation of the coordinate system, we use ZYX Euler angles (Wittbrodt et al. 2006), and the transformation of coordinates is performed by means of homogenous transformations (Craig 1989). Position and orientation of base $\{\}\hat{}$ with respect to the global system {} are defined by the vector of position

$$\widehat{\mathbf{r}} = \begin{bmatrix} \widehat{x}(t) \\ \widehat{y}(t) \\ \widehat{z}(t) \end{bmatrix} \tag{1a}$$

and orientation

$$\widehat{\mathbf{\Phi}} = \begin{bmatrix} \widehat{\psi}(t) \\ \widehat{\theta}(t) \\ \widehat{\varphi}(t) \end{bmatrix}, \tag{1b}$$

where it is assumed that $\widehat{x}(t)$, $\widehat{y}(t)$, $\widehat{z}(t)$, $\widehat{\psi}(t)$, $\widehat{\theta}(t)$, $\widehat{\varphi}(t)$ are known functions of time and can define base motion caused by sea waves, sea currents and wind.

Transformation of coordinates from system $\{\}\hat{}$ to system {} is carried out according to the following formula:

$$\mathbf{r} = \widehat{\mathbf{r}} + \widehat{\mathbf{R}}\widehat{\mathbf{r}}', \tag{2}$$

where $\widehat{\mathbf{r}}'$ is the vector of coordinates in system $\{\}\hat{}$, $\widehat{\mathbf{R}} = \mathbf{R}_{\widehat{\psi}}\mathbf{R}_{\widehat{\theta}}\mathbf{R}_{\widehat{\varphi}}$ is the rotation matrix, $\mathbf{r}$ is the position

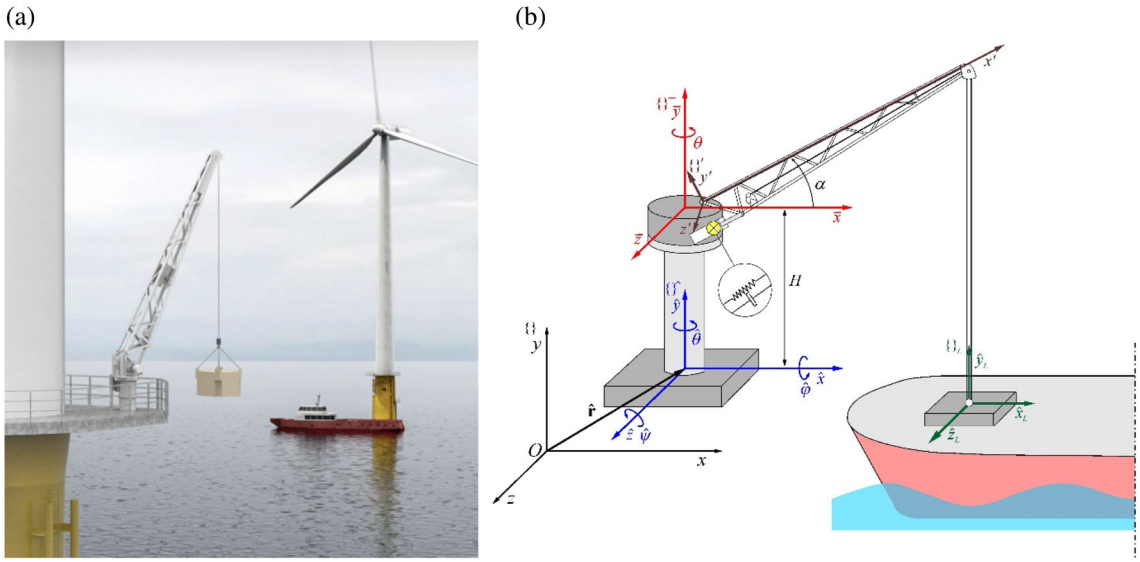


**Fig. 1** The crane analysed: **a** general view and **b** model assumed

vector in global system $\{\}$, $\mathbf{R}_{\widehat{\psi}} = \begin{bmatrix} c\widehat{\psi} & -s\widehat{\psi} & 0 \\ s\widehat{\psi} & c\widehat{\psi} & 0 \\ 0 & 0 & 1 \end{bmatrix}$, $\mathbf{R}_{\widehat{\theta}} = \begin{bmatrix} c\widehat{\theta} & 0 & s\widehat{\theta} \\ 0 & 1 & 0 \\ -s\widehat{\theta} & 0 & c\widehat{\theta} \end{bmatrix}$, $\mathbf{R}_{\widehat{\varphi}} = \begin{bmatrix} 1 & 0 & 0 \\ 0 & c\widehat{\varphi} & -s\widehat{\varphi} \\ 0 & s\widehat{\varphi} & c\widehat{\varphi} \end{bmatrix}$.

Both in the formulae above and for further considerations, the following notation is assumed:

$$c\gamma = \cos\gamma, \tag{3a}$$

$$s\gamma = \sin\alpha\gamma, \tag{3b}$$

where $\gamma \in \{\widehat{\psi}, \widehat{\theta}, \widehat{\varphi}\}$.

Using homogenous transformations, relationship (2) can be written in the form

$$\underline{\mathbf{r}} = \mathbf{B}\underline{\widehat{\mathbf{r}}}', \tag{4}$$

where $\underline{\mathbf{r}} = \begin{bmatrix} \mathbf{r} \\ 1 \end{bmatrix}$, $\mathbf{B} = \begin{bmatrix} \widehat{\mathbf{R}} & \widehat{\mathbf{r}} \\ 0 & 1 \end{bmatrix}$, $\underline{\widehat{\mathbf{r}}}' = \begin{bmatrix} \widehat{\mathbf{r}}' \\ 1 \end{bmatrix}$.

Homogenous transformations enable the transformations between coordinate systems to be performed by only one mathematical operation, namely multiplication of a matrix by a vector (formula 4). In the classical approach (formula 2), two operations are necessary: multiplication of a matrix by a vector and sum of vectors. Although, in the latter, the dimension of matrices and vectors is 3 and is smaller than when homogenous transformations are used, the use of formula (4) considerably facilitates the description of the transformation of coordinates.

Coordinates from system $\{\}^-$, assigned to the rotary platform of the crane, to system $\{\ \}\hat{}$ and to the global system, are transformed by means of the following formulae:

$$\underline{\widehat{\mathbf{r}}} = \mathbf{P}\underline{\overline{\mathbf{r}}}, \tag{5a}$$

$$\underline{\mathbf{r}} = \mathbf{B}\underline{\widehat{\mathbf{r}}} = \mathbf{BP}\underline{\overline{\mathbf{r}}} = \mathbf{D}\underline{\overline{\mathbf{r}}}, \tag{5b}$$

where $\mathbf{P} = \begin{bmatrix} c\theta & 0 & s\theta & 0 \\ 0 & 1 & 0 & H \\ -s\theta & 0 & c\theta & 0 \\ 0 & 0 & 0 & 1 \end{bmatrix}$, $H$ is the distance between systems $\{\ \}\hat{}$ and $\{\}^-$ (Fig. 1b), $\mathbf{D} = \mathbf{BP}$, $\underline{\overline{\mathbf{r}}}$ is the coordinate vector in system $\{\}^-$ assigned to the rotary part of the crane, and $\theta$ is the rotation angle of system $\{\}^-$ with respect to system $\{\ \}\hat{}$ (about axis$\widehat{y}$), which is the rotation angle of the crane platform in relation to the base (platform or vessel).

The truss boom is divided into nodes and members (Fig. 2). It is assumed that the nodes reflect mass features of the truss, while the members reflect its damping and stiffness features. The nodes are denoted by $(i)$ and are numbered from 1 to $n$.

The position and orientation coordinates of truss node $i-$th (Fig. 2a) with respect to system $\{\}^-$ form the vector of generalised coordinates describing the motion with respect to the rotary platform

$$\mathbf{q}_i = \begin{bmatrix} \overline{\mathbf{r}}_i \\ \mathbf{\Phi}_i \end{bmatrix}, \tag{6}$$

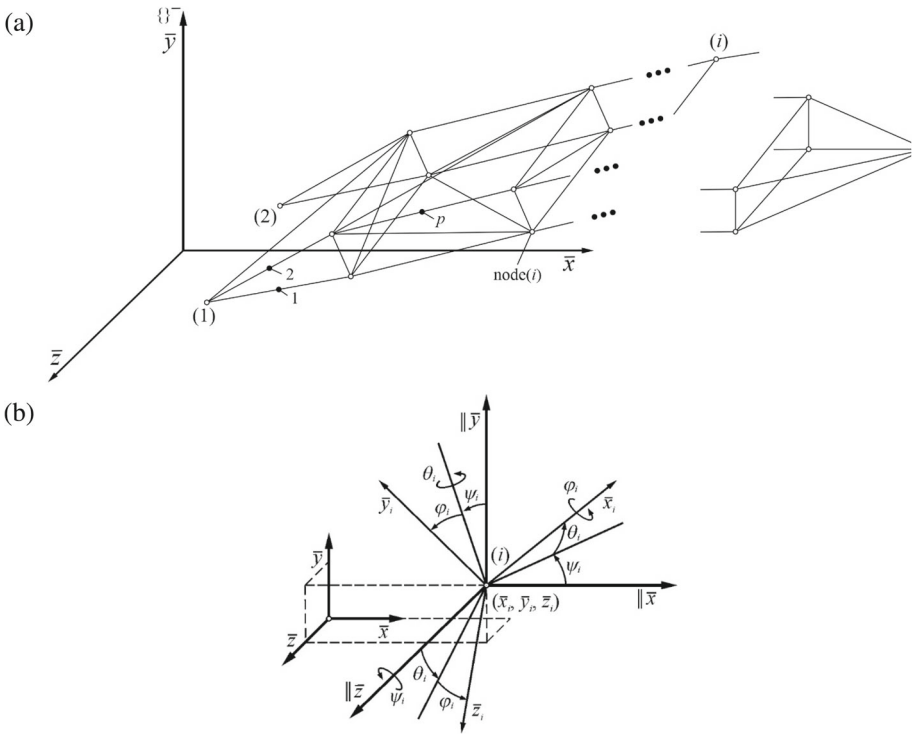


**Fig. 2** Truss boom: **a** members and nodes ( ); **b** translation $(\overline{x}_i, \overline{y}_i, \overline{z}_i)$ and rotation $(\psi_i, \theta_i, \varphi_i)$ coordinates of node $(i)$

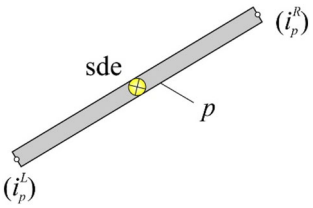


**Fig. 3** The truss member and nodes at its ends, ⊕—spring–damping element (sde)

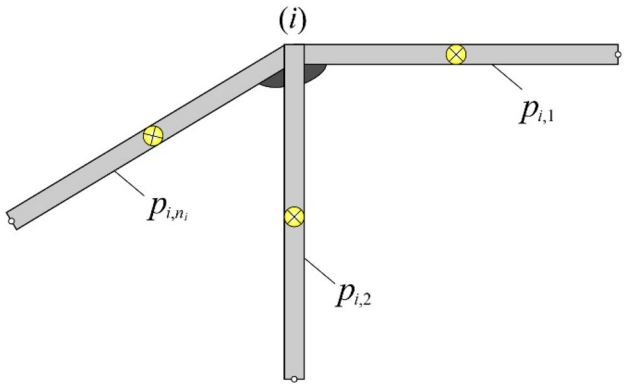


**Fig. 4** Members $p_{i,1}, \ldots, p_{i,n_i}$ connecting at node $(i)$

where $\overline{\mathbf{r}}_i$ are coordinates of a truss node in system$\{\}^-$, and $\mathbf{\Phi}_i = \begin{bmatrix} \psi_i \\ \theta_i \\ \varphi_i \end{bmatrix}$ are ZYX Euler angles (Craig 1989) defining orientation of the node axis with respect to system $\{\}^-$ (Fig. 2b).

When the crane is unloaded, angles $\psi_i$ of the nodes are inclined to axis $\overline{x}$ of system $\{\}^-$ at the same angle $\psi_i = \psi_J = \alpha$ (Fig. 1), and angles $\theta_i = \varphi_i = 0$ for $i = 1, \ldots, n$.

Truss members are numbered from 1 to $m$. For each member $p = 1, \ldots, m$ numbers $(i_p^L)$ and $(i_p^R)$ define nodes at the ends of the member (Fig. 3).

The model assumes that the ends of the members meeting at node $(i)$ are rigidly connected (Fig. 4). This causes translational and rotational displacements of the ends of the members connected at node $(i)$ to be equal.

Generalised coordinates of the model of the crane shown in Fig. 1b are the components of the following vector:

$$\mathbf{u} = \begin{bmatrix} \mathbf{q}_1 \\ \vdots \\ \mathbf{q}_n \\ \theta \\ \mathbf{r}_L \\ \varphi_0 \end{bmatrix} \begin{matrix} -\text{coordinates of node (1)} \\ \vdots \\ -\text{coordinates of node } (n) \\ -\text{rotation angle of the boom platform} \\ -\text{vector of coordinates of the load (mass } m_L) \\ -\text{winch drum rotation angle} \end{matrix} \tag{7}$$

where $\mathbf{r}_L = \begin{bmatrix} x_L & y_L & z_L \end{bmatrix}^T$.

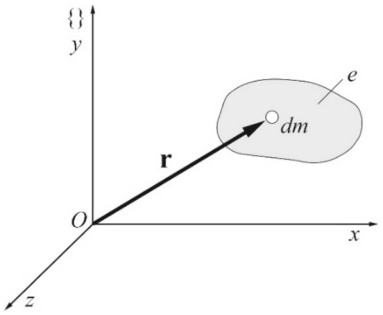


**Fig. 5** Element $e$ and mass $dm$

Thus, the vector of generalised coordinates $\mathbf{u}$ of the system consists of

$$N = 6n + 1 + 3 + 1 = 6n + 5 \tag{8}$$

components.

## 3 Equations of motion of the crane

To formulate the equations of motion, the formalism based on the Lagrange equations of the second order, presented in detail by Wittbrodt et al. (2006) and Adamiec-Wójcik et al. (2019), is used. The equations can be written in the following form:

$$\frac{d}{dt}\frac{\partial E}{\partial \dot{u}_i} - \frac{\partial E}{\partial u_i} + \frac{\partial V}{\partial u_i} + \frac{\partial D}{\partial \dot{u}_i} = Q_i \quad i = 1 \ldots N, \tag{9}$$

where $E$ is the kinetic energy of the system, $V$ is its potential energy, $D$ denotes dissipation of the energy of the system, $u_i$ is the $i$th component of the vector of the generalised coordinates, and $Q_i$ is the $i$th generalised force.

The kinetic energy of an element (Fig. 5) can be presented in the form

$$E_e = \frac{1}{2}\int_{m_e} \dot{\underline{\mathbf{r}}}^T \dot{\underline{\mathbf{r}}} dm = \frac{1}{2}\int_{m_e} tr(\dot{\underline{\mathbf{r}}}\dot{\underline{\mathbf{r}}}^T) dm, \tag{10}$$

where $e$ and $m_e$ are the number and mass of the element, respectively, $\underline{\mathbf{r}} = \begin{bmatrix} \mathbf{r} \\ 1 \end{bmatrix}$, and $tr(\mathbf{A})$ denotes the trace of matrix $\mathbf{A}$.

Due to relation (5b), the kinetic energy of the rotary platform of the crane is defined by the expression

$$E_\theta = \frac{1}{2} tr \int_{m_\theta} (\dot{\mathbf{D}}\dot{\underline{\mathbf{r}}}^T \dot{\underline{\mathbf{r}}}\dot{\mathbf{D}}) dm = \frac{1}{2} tr\left(\dot{\mathbf{D}}\mathbf{H}_\theta \dot{\mathbf{D}}^T\right), \tag{11}$$

where $\mathbf{H}_\theta = \int_{m_\theta} (\dot{\underline{\mathbf{r}}}^T \dot{\underline{\mathbf{r}}}) dm$ is the pseudo-inertial matrix and $m_\theta$ is the mass of the rotary platform.

For nodes $(1) \ldots (n)$ of the truss, the following can be written:

$$E_i = \frac{1}{2}\int_{m_i} tr(\dot{\underline{\mathbf{r}}}\dot{\underline{\mathbf{r}}}^T) dm, \tag{12}$$

where $\underline{\mathbf{r}} = \mathbf{D}\mathbf{A}_i\underline{\mathbf{r}}' = \mathbf{B}_i\underline{\mathbf{r}}'$, $\mathbf{D}$ defined in (5), $\mathbf{A}_i = \begin{bmatrix} \mathbf{R}_i & \bar{\mathbf{r}}_i \\ 0 & 1 \end{bmatrix}$ is the transformation matrix from the system assigned to node$(i)$, which is$\{i\}$, to system$\{\}^-$; $\bar{\mathbf{r}}_i$ is defined in (6); $\mathbf{R}_i = \mathbf{R}_i^\psi \mathbf{R}_i^\varphi \mathbf{R}_i^\theta$, matrices $\mathbf{R}_i^\psi$, $\mathbf{R}_i^\varphi$, $\mathbf{R}_i^\theta$ are defined as in (2) having assumed $\widehat{\psi} = \psi_i$, $\widehat{\theta} = \theta_i$, $\widehat{\varphi} = \varphi_i$; $\mathbf{B}_i = \mathbf{D}\mathbf{A}_i$; $\underline{\mathbf{r}}'$ are local coordinates with respect to the system of node$(i)$; $m_i$ is the mass applied to node$(i)$, which equals the halves of the mass of each member $p_{i,1}, \ldots, p_{i,n_i}$ meeting at this node (Fig. 4).

According to (10) and (12), kinetic energy $E_i$ can be presented as follows:

$$E_i = \frac{1}{2} tr\left(\dot{\mathbf{B}}_i \mathbf{H}_i \dot{\mathbf{B}}_i^T\right), \tag{13}$$

where $\mathbf{H}_i = \int_{m_i} (\dot{\underline{\mathbf{r}}}'^T \dot{\underline{\mathbf{r}}}') dm$ is the pseudo-inertial mass matrix of node $(i)$.

To calculate elements of matrix $\mathbf{H}_i$ the location of nodes and members of the truss in the no-load conditions should be taken into account. Let angles $\alpha_p$ and $\beta_p$ define the orientation of member $p$ with respect to axes of nodes $(i) = (w_p^L)$ and $(j) = (w_p^R)$ at its ends (Fig. 6).

Angles $\alpha_p$ and $\beta_p$ are constant in coordinate systems $\{i\}$ and $\{j\}$. The transformation (rotation) matrix from system $\{p\}'$ assigned to member $p$ to the systems assigned to nodes $(i)$ and $(j)$ can be written in the form

$$\mathbf{U}_p = \begin{bmatrix} c\alpha_p & -s\alpha_p & 0 \\ s\alpha_p & c\alpha_p & 0 \\ 0 & 0 & 1 \end{bmatrix} \begin{bmatrix} c\beta_p & 0 & s\beta_p \\ 0 & 1 & 0 \\ -s\beta_p & 0 & c\beta_p \end{bmatrix}. \tag{14}$$

These are matrices with constant elements.

Transformation of vector $\underline{\mathbf{r}}_p'$ defined in $\{p\}'$ to the base coordinate system can be performed using the formula

$$\underline{\mathbf{r}} = \mathbf{B}_i \mathbf{L}_p \underline{\mathbf{r}}_p' \tag{15a}$$

or

$$\underline{\mathbf{r}} = \mathbf{B}_j \mathbf{L}_p \left(-\underline{\mathbf{r}}_p'\right) = -\mathbf{B}_j \mathbf{L}_p \underline{\mathbf{r}}_p', \tag{15b}$$

where $\mathbf{L}_p = \begin{bmatrix} \mathbf{U}_p & 0 \\ 0 & 1 \end{bmatrix}$.

To calculate matrix $\mathbf{H}_i$ from formula (11), partial matrices of half of the members connected at this node, as in Fig. 4,

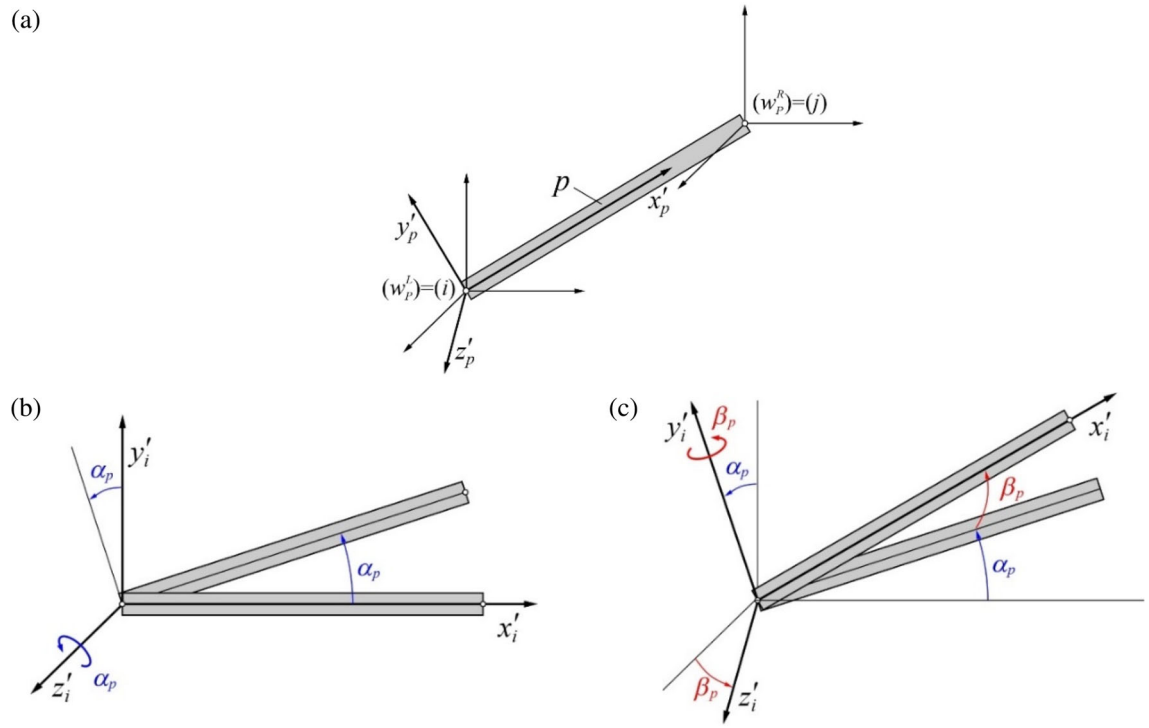


**Fig. 6** **a** Member $p$ with nodes $(i)$ and$(j)$, **b** rotation angle $\alpha_p$, **c** rotation angle $\beta_p$

have to be summed obtaining the following:

$$E_i = \frac{1}{2}\sum_{k=1}^{n_i}\int_{m_{p_{i,k}}/2} tr(\dot{\mathbf{B}}_i \mathbf{L}_{p_{i,k}} \underline{\mathbf{r}}'_{p_{i,k}} \underline{\mathbf{r}}'^{T}_{p_{i,k}} \mathbf{L}^T_{p_{i,k}} \dot{\mathbf{B}}_i^T) dm = \frac{1}{2} tr\left(\dot{\mathbf{B}}_i \mathbf{H}_i \dot{\mathbf{B}}_i^T\right), \tag{16}$$

where $\mathbf{H}_i = \sum_{k=1}^{n_i} \mathbf{L}_{p_{i,k}} \left(\int_{m_{p_{i,k}}/2} \underline{\mathbf{r}}'_{p_{i,k}} \underline{\mathbf{r}}'^{T}_{p_{i,k}} dm\right) \mathbf{L}^T_{p_{i,k}}$.

It is assumed that the half-length of member $p_{i,k}$ applies its mass to node $(i)$, while the other half of the mass is applied to node $(j)$.

When the cross-section of member $p_{i,k}$ is constant, it can be assumed that

$$\mathbf{H}_{p_{i,k}} = \begin{bmatrix} m_{p_{i,k}}(l^0_{p_{i,k}})^2/24 & 0 & 0 & m_{p_{i,k}}(l^0_{p_{i,k}})^2/8 \\ 0 & J^y_{p_{i,k}} & 0 & H \\ 0 & 0 & J^z_{p_{i,k}} & 0 \\ m_{p_{i,k}}(l^0_{p_{i,k}})^2/8 & 0 & 0 & m_{p_{i,k}}(l^0_{p_{i,k}})^2/24 \end{bmatrix}, \tag{17}$$

where $J^y_{p_{i,k}} = A_{p_{i,k}}\rho\int_0^{l^0_{p_{i,k}}/2}(z')^2 dm, J^z_{p_{i,k}} = A_{p_{i,k}}\rho\int_0^{l^0_{p_{i,k}}/2}(y')^2 dm$, $A_{p_{i,k}}$ is the cross-section area of member $p_{i,k}$, $\rho$ is the material density of the member, and $l^0_{p_{i,k}}$ is the length of unloaded member $p_{i,k}$. Elements of matrices $\mathbf{H}_{p_{i,k}}$ and $\mathbf{H}_i$ are constant.

Kinetic energy of the whole boom can be written as follows:

$$E_J = \sum_{i=1}^{n} E_i, \tag{18}$$

where $E_i$ defined in (16) depends on $\mathbf{q_i}$, $\theta$ and $t$.

Kinetic energy of the drum winch is calculated as follows:

$$E_D = \frac{1}{2} J_D \dot{\varphi}_D^2, \tag{19}$$

where $J_D$ is the mass moment of inertia of the drum winch.

Kinetic energy of the load is calculated according to the following formula:

$$E_L = \frac{1}{2} m_L \dot{\mathbf{r}}_L^T \dot{\mathbf{r}}_L, \tag{20}$$

where $m_L$ is the mass of the load.

According to (7), components of vector $\mathbf{r}_L$ are generalised coordinates when the load is in the air. When the load rests on the deck of the supply vessel, its generalised coordinates are assumed to be known and determined by the movement of the supply vessel, which means that

$$\mathbf{r}_L = \widehat{\mathbf{r}}_L(t) \tag{21}$$

is a known function of time.

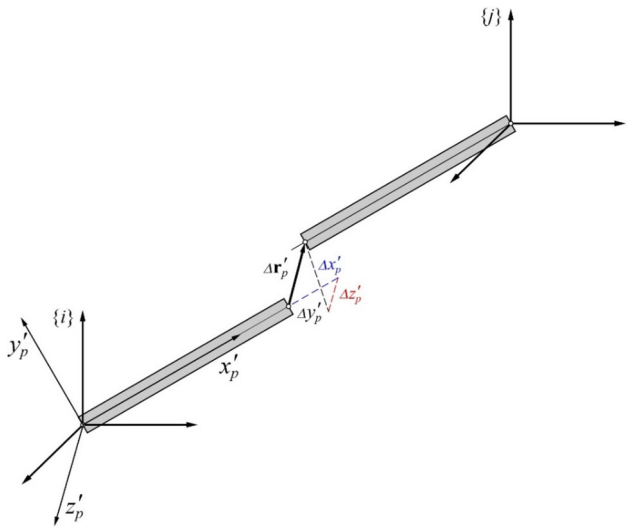


**Fig. 7** Translational deformation of member $p$

Total kinetic energy equals

$$E = E_J + E_\theta + E_L. \tag{22}$$

Energy of translational deformation of sde $p$ from Fig. 3 is calculated as follows:

$$V_p^t = \frac{1}{2}\Delta\mathbf{r}_p^{'T}\mathbf{C}_p^t\Delta\mathbf{r}_p^{'}, \tag{23}$$

where $\mathbf{C}_p^t = \begin{bmatrix} c_{p,x'} & 0 & 0 \\ 0 & c_{p,y'} & 0 \\ 0 & 0 & c_{p,z'} \end{bmatrix}$, $\Delta\mathbf{r}_p^{'}$ is the difference of displacements at the middle of the member $p$, and $x_p^{'} = l_p^0/2$ (Fig. 7).

Bearing in mind the previously introduced notation, it can be written that $\Delta\mathbf{r}_p^{'}$ is the projection of the difference of relative displacements $\bar{\mathbf{r}}_p^R$ and $\bar{\mathbf{r}}_p^L$ on the direction of the part of member $p$ assigned to node $(i)$

$$\Delta\mathbf{r}_p^{'} = \left(\mathbf{R}_i\mathbf{U}_p\right)^T\left(\bar{\mathbf{r}}_p^R - \bar{\mathbf{r}}_p^L\right) = \mathbf{R}_{i,p}^T\left(\bar{\mathbf{r}}_p^R - \bar{\mathbf{r}}_p^L\right), \tag{24}$$

where $\bar{\mathbf{r}}_p^R = \bar{\mathbf{r}}_j + \mathbf{R}_{j,p}\mathbf{r}_{p,R}^{'}$, $\mathbf{R}_{j,p} = \mathbf{R}_j\mathbf{L}_p$, $\mathbf{r}_{p,R}^{'} = \left[-l_p^0/2\ 0\ 0\right]^T$, $\bar{\mathbf{r}}_p^L = \bar{\mathbf{r}}_j + \mathbf{R}_{i,p}\mathbf{r}_{p,L}^{'}$, $\mathbf{R}_{i,p} = \mathbf{R}_i\mathbf{U}_p$, and $\mathbf{r}_{p,L}^{'} = \left[l_p^0/2\ 0\ 0\right]^T$.

Energy of rotational deformation of sde $p$ can be presented in the form

$$V_p^r = \frac{1}{2}\Delta\mathbf{\Phi}_p^{'T}\mathbf{C}_p^r\Delta\mathbf{\Phi}_p^{'}, \tag{25}$$

where $\mathbf{C}_p^r = \begin{bmatrix} c_{p,\psi} & 0 & 0 \\ 0 & c_{p,\theta} & 0 \\ 0 & 0 & c_{p,\varphi} \end{bmatrix}$, and $\Delta\mathbf{\Phi}_p^{'}$ is the difference in rotation angles between the halves of member $p$ connected by means of the spring–damping element, expressed in member coordinate system $\{p\}'$.

Vector $\Delta\mathbf{\Phi}_p^{'}$ can be calculated from the relation

$$\Delta\mathbf{\Phi}_p^{'} = \mathbf{\Phi}_{p,R}^{'} - \mathbf{\Phi}_{p,L}^{'}, \tag{26}$$

where $\mathbf{\Phi}_{p,R}^{'} = \mathbf{R}_{j,p}^T\mathbf{\Phi}_j$, $\mathbf{\Phi}_{p,L}^{'} = \mathbf{R}_{i,p}^T\mathbf{\Phi}_i$.

The energy of spring deformation of sde $p$ is the sum of the quantities from (23) and (25), and the energy of spring deformation of the whole truss is

$$V = \sum_{p=1}^{m}\left(V_p^t + V_p^r\right). \tag{27}$$

The method of calculating the stiffness coefficients of sdes is based on the approach described by Kruszewski et al. (1975) and Wittbrodt et al. (2006). If member $p$ is a homogenous beam with length $l_p^0$, then the stiffness coefficients of sde can be expressed by the following formulae:

$$c_{p,x'} = c_{p,1} = \frac{E_pA_p}{l_p^0}\ \text{longitudinal stiffness coefficient,} \tag{28a}$$

$$\left.\begin{aligned} c_{p,y'} = c_{p,2} &= \frac{12E_pI_p^y}{\left(l_p^0\right)^3} \\ c_{p,z'} = c_{p,3} &= \frac{12E_pI_p^z}{\left(l_p^0\right)^3} \end{aligned}\right\}$$

shear stiffness coefficient for Bernouli beam, (28b)

$$\left.\begin{aligned} c_{p,y'} = c_{p,2} &= \frac{G_pA_p}{l_p^0} \\ c_{p,z'} = c_{p,3} &= \frac{G_pA_p}{l_p^0} \end{aligned}\right\}$$

shear stiffness coefficient for Timoszenko beam, (28c)

$$\left.\begin{aligned} c_{p,\psi} = c_{p,4} &= \frac{E_pI_p^y}{l_p^0} \\ c_{p,\theta} = c_{p,5} &= \frac{E_pI_p^z}{l_p^0} \end{aligned}\right\}\ \text{bending stiffness coefficients,} \tag{28d}$$

$$c_{p,\varphi} = c_{p,6} = \frac{G_pI_p^x}{l_p^0}\ \text{torsional stiffness coefficient,} \tag{28e}$$

where $E_p$ is the elasticity modulus, $A_p$ is the cross-section area, $G_p$ is the shear modulus, and $I_p^x$, $I_p^y$, $I_p^z$ are second moment of inertia with respect to axes $x_p^{'}$, $y_p^{'}$, $z_p^{'}$, respectively.

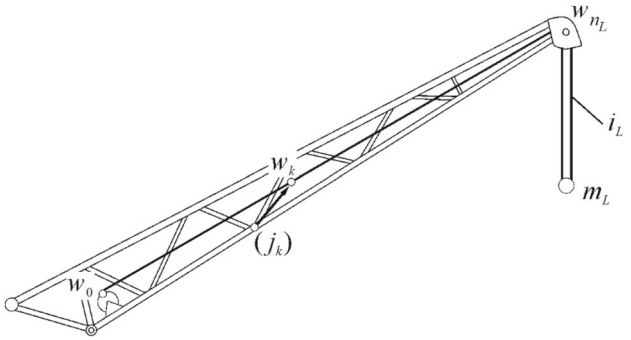


**Fig. 8** Winch rope system

The rope connecting the load with the winch is also a flexible element. The energy of elastic deformation of the rope can be presented as follows:

$$V_r = \frac{1}{2} c_r \Delta r^2, \tag{29}$$

where $c_r$ is the stiffness coefficient of the rope, and $\Delta r$ is the deformation (elongation) of the rope which can be calculated as follows:

$$\Delta r = l - l_0 + \varphi_0 r_D, \tag{30}$$

where $l$ is the actual length of the rope, $l_0$ is the initial length of the rope, and $r_D$ is the radius of the winch drum.

The actual length of the rope can be calculated from the formula

$$l = \sum_{k=1}^{n_L} \|\mathbf{r}_k - \mathbf{r}_{k-1}\| + i_L \|\mathbf{r}_{n_L} - \mathbf{r}_L\|, \tag{31}$$

where $\|\mathbf{r}\|$ is the length of vector $\mathbf{r}$, $i_L$ is the ratio of the rope system on the section $\mathbf{r}_{n_L}\mathbf{r}_L$, $n_L$ is the number of points on the boom the rope passes through, $\mathbf{r}_k$ is the vector of coordinates of point $w_k$ which the rope passes through, and $\mathbf{r}_0$ is the vector of coordinates of point $w_0$ on the perimeter of the winch drum**.**

If $\mathbf{r}_k^{'}$ are local coordinates of point $w_k$ with respect to the local coordinate system of node $(j_k)$ (Fig. 8), then

$$\|\mathbf{r}_k - \mathbf{r}_{k-1}\|^2 = \left[\mathbf{r}_k - \mathbf{r}_{k-1}\right]^T \left[\mathbf{r}_k - \mathbf{r}_{k-1}\right], \tag{32}$$

where $\mathbf{r}_k = \mathbf{B}_{jk}\mathbf{r}_k^{'}$ and

$$\|\mathbf{r}_{n_L} - \mathbf{r}_L\|^2 = \left[\mathbf{r}_{n_L} - \mathbf{r}_L\right]^T \left[\mathbf{r}_{n_L} - \mathbf{r}_L\right]. \tag{33}$$

When considering the potential energy of elastic deformation of the system, one must also take into account the elastic deformation energy of the cylinder or the rope-lowering system (Fig. 9).

The coordinates of point $A$ in system $\{\}^{-}(\overline{\mathbf{r}}_A = \left[\overline{x}_A\ \overline{y}_A\ \overline{z}_A\right]^T)$ and the local coordinates of the connection point with the jib ($\mathbf{r}_{is}^{'}$ in the local coordinate system of node $(i_s)$) are assumed to be known. The deformation energy of the boom or the luffing rope system may be presented in the form

$$V_s = \frac{1}{2} c_s \Delta_s^2, \tag{34}$$

where $c_s$ is the stiffness coefficient and $\Delta_s$ is the deformation which can be calculated from the following relation:

$$\Delta_s = \|\overline{\mathbf{r}}_{is} - \overline{\mathbf{r}}_A\| - L_s^0, \tag{35}$$

where $\overline{\mathbf{r}}_{is} = \mathbf{B}_{is}\mathbf{r}_{is}^{'}$, $L_s^0$ is the initial length of the cylinder or rope (with no load on the system).

The total deformation energy of the system can be represented as

$$V_f = V_J + V_r + V_s. \tag{36}$$

In a similar way, it is possible to slightly modify the relations (22)–(36) to calculate the energy dissipation of the system (Kruszewski et al. 1975)

$$D_f = D_J + D_r + D_s. \tag{37}$$

It is important to note that the stiffness and damping coefficients ($c_r$ and $b_r$ respectively) of the rope depend on the extended length of the rope. Similarly, the stiffness and damping coefficients of the luffing system may change.

The equations of motion of the crane are derived according to Eq. (9), taking into account the relation on the kinetic energy (22) and the relations on the energy of elastic deformation and energy dissipation (36, 37). Having considered gravity forces and moments $M_\theta$ (platform rotation) and $M_D$ (winch drum rotation), the equations of motion form a system of $N$ non-linear ordinary differential equations of the second order in the following form:

$$\mathbf{M}(\mathbf{q})\ddot{\mathbf{q}} = \mathbf{f}(t, \mathbf{q}, \dot{\mathbf{q}}). \tag{38}$$

The Runge–Kutta method of the fourth order or the Newmark method with the iterative procedure necessary due to the non-linearity of Eq. (38) are used to differentiate the equations of motion (Wittbrodt et al. 2006).

The procedures of the integration of the above equations can be accelerated when the specific form of matrix $\mathbf{M}$ is

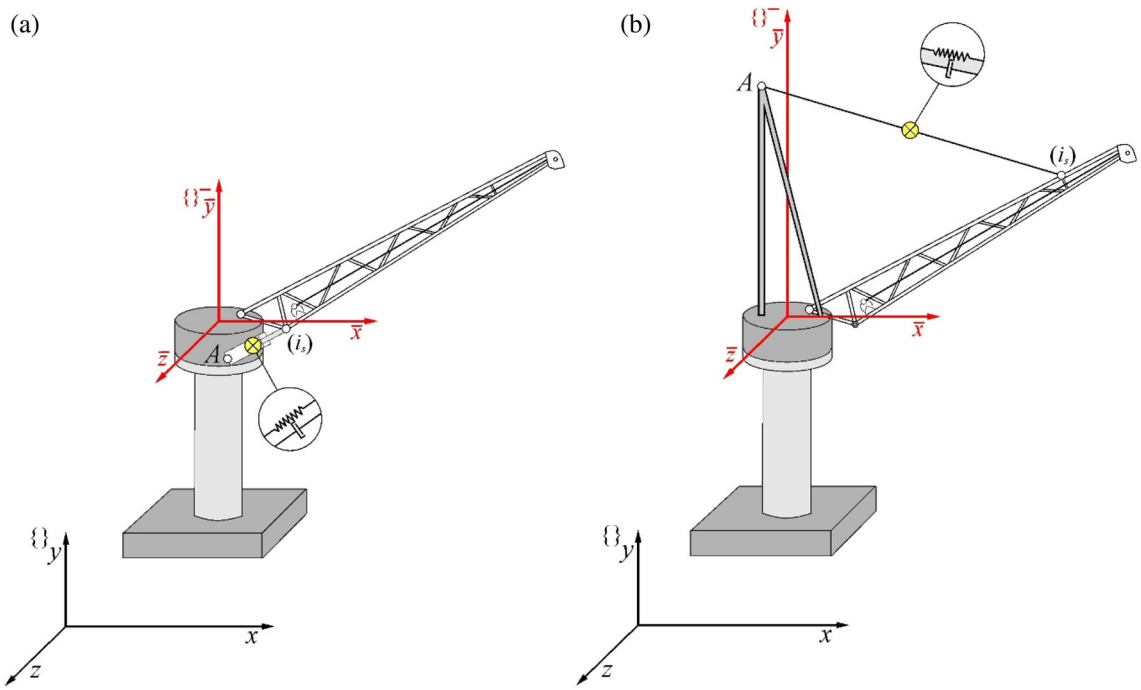


**Fig. 9** Luffing system: **a** with a cylinder and **b** with a rope system

taken into account

$$\mathbf{M}(\mathbf{q}) = \begin{bmatrix} \mathbf{M}_{\theta\theta} & \mathbf{M}_{\theta J} & \mathbf{M}_{\theta L} & \mathbf{M}_{\theta D} \\ & \mathbf{M}_{JJ} & \mathbf{M}_{JL} & \mathbf{M}_{JD} \\ & SYM & \mathbf{M}_{LL} & \mathbf{M}_{LD} \\ & & & \mathbf{M}_{DD} \end{bmatrix}, \tag{39}$$

where $\mathbf{M}_{JJ} = \begin{bmatrix} \mathbf{M}_1 & 0 & \cdots & 0 & \cdots & 0 \\ 0 & \mathbf{M}_2 & \cdots & 0 & \cdots & 0 \\ \vdots & \vdots & & \vdots & & \vdots \\ 0 & 0 & \cdots & \mathbf{M}_i & \cdots & 0 \\ \vdots & \vdots & & \vdots & & \vdots \\ 0 & 0 & \cdots & 0 & \cdots & \mathbf{M}_n \end{bmatrix}$, $\mathbf{M}_i = (m_i)_{j,k=1}^{6}$, $i = 1, 2, \ldots, n$.

The block-diagonal form of matrix$\mathbf{M}_{JJ}$, obtained due to the assumption that coordinates of nodes in system $\{\}^-$ are independent, makes it possible to accelerate the calculations.

## 4 Verification and validation of the simulation model

The spatial mathematical model of the dynamics of the lattice crane presented in the previous section has been implemented in a Delphi environment. Verification of the model and its computer implementation consists in comparing the static deflections of the boom structure obtained by means of our own model with those calculated using the Microsoft ROBOT package for three cases of the boom end load:

(P1) vertical force $F_y$ in the range from 10 to 30 kN,
(P2) horizontal force $F_z$ in the range from 10 to 30 kN,
(P3) simultaneous load with vertical force $F_y = 20$ kN and horizontal force $F_z = 30$ kN for different angles of the truss inclination $\alpha$ in the range from $0^o$ to $80^o$,

and a comparison of the values of natural frequencies of the boom obtained by both models.

Verification calculations have been carried out for the lattice boom, which is a structural element of the lightweight service crane manufactured by Protea and intended for wind platforms (Fig. 10). The boom structure consists of 4 beams with a square cross-section of 100 × 100 × 6.3 mm, connected alternately by diagonal crosses with a circular cross-section Ø51 × 4 mm. The ends of the upper and lower leading beams are connected with four elements substituting the end of the boom by means of parameters corresponding to the stiff tip of the leading beams. In practice, this substitution means stiffening the structure at this point. The most important design, geometrical and mass parameters of the truss are presented in Table 1.

For the calculations in this section, it is assumed that at nodes $(A_1)$ and $(A_2)$, there are sliding supports, while nodes $(B_1)$ and $(B_2)$ are fixed. Moreover, vertical and horizontal forces are applied at node $(G)$. Gravity is not included in the calculations.

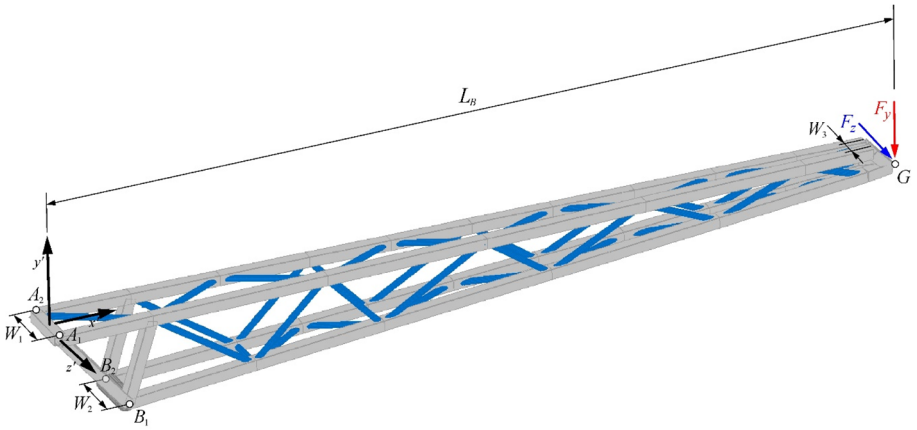


**Fig. 10** Design of the lattice boom

The material density of the truss construction elements is taken as $\rho = 7850$ kg/m$^3$, and the strength parameters are: Young modulus $E = 210$ GPa, Kirchoff's modulus of shear elasticity $G = E/[2(1 + \upsilon]$, and $\nu = 0.3$.

Tables 2 and 3 show the results of vertical $U_y$ and horizontal $U_z$ deflections of the jib after loading its end with vertical $F_y$ and/or horizontal $F_z$ forces, obtained in Microsoft Robot and our own model. The tables also contain absolute $\Delta$ and relative $\delta$ differences between the two. In the case of calculating relative values, the reference value is the result obtained in Microsoft Robot.

By analysing the calculation results and their differences shown in Tables 2 and 3, it can be concluded that in both cases of the boom end load with vertical (P1) and horizontal (P2) forces, both models give similar deflection values. The relative difference does not exceed 0.6%. Slightly bigger deflections are obtained by the authors' own model. In the case of a load with a vertical force, the difference remains at a similar level, namely 0.35%. On the other hand, when the value of the load with the horizontal force increases, the difference in deflections between the models increases, but remains at an acceptable level.

Larger differences between the deflection values along with the change of the boom inclination angle can be noticed by analysing the calculation results presented in Table 4. The increase of the boom inclination angle $\alpha$ in the range of $\langle 0°; 60°\rangle$, with a constant value of the load force, changes relative difference $\delta U_\alpha$ from $-0.03$ to $-0.83$%. The results presented in Table 4 are obtained for case P1.

The results concerning the natural frequencies of the boom structure calculated by means of the authors' own model and Microsoft Robot software package are presented in Table 5. Good consistency of the calculation results is obtained for the first 5 frequency values. Absolute difference $\Delta\omega_i$ does not exceed 0.25 Hz, and relative difference $\delta\omega_i$ is lower than 1%. Slightly higher frequency values are obtained in our own model.

## 5 Application of the model

One of the important tasks that must be performed before operating offshore cranes in real conditions is checking their resistance to adverse environmental conditions. Sea waves and the impact of wind are among the most important. Before starting the production of offshore cranes, constructors must make a series of engineering calculations that will confirm the strength of individual structural elements. For many years, guidelines have also been developed in the form of standards that enable the verification of design assumptions. In the case of offshore cranes, there are static calculations taking into account the influence of individual factors on the structure. The model of the dynamics of the truss crane proposed extends these possibilities, because in addition to performing static calculations, it enables simulations taking into account base motion, motion of the delivery vessel, and various types of drives (electric, hydraulic) for transportation (load lifting, column rotation).

This section presents the results of simulations carried out with the use of the authors' own programme, performed for a spatial model of a service crane with a capacity of 2000 kg intended for servicing wind platforms. Detailed design parameters of the crane jib are included in the section concerning verification of the lattice jib model (Table 1, Fig. 10). In the model, it is assumed that the boom on the rotating platform (column) is mounted at point $O_1(\overline{x}_{O_1} = 0.190\,\text{m}; \overline{y}_{O_1} = 0.820\,\text{m}; \overline{z}_{O_1} = 0)$. In addition, the crane's reach change mechanism is a single cylinder connected to the column at point $A(\overline{x}_A = 0.345\,\text{m}; \overline{y}_A = 0.102\,\text{m}; \overline{z}_A = 0)$, and to the boom at point $B(x'_B = 0.683\,\text{m}; y'_B = -0.806\,\text{m}; \overline{z}_B = 0)$. The most important parameters of the actuator are presented in Table 6.

The crane is equipped with an electric winch. The parameters of the winch and the rope system are presented in Table 7. An additional electric drive is used for the rotation of the crane column.

**Table 1** Design, geometrical and mass parameters of the boom

| Parameter | Symbol | Unit | Value |
|---|---|---|---|
| Length of the truss | $L_B$ | (m) | 8.368 |
| Width of the truss at the support point | $W_1$ | (m) | 0.510 |
| Width of the truss at the point of restraint | $W_2$ | (m) | 0.510 |
| Width of the truss at the end of the leading beams | $W_3$ | (m) | 0.150 |
| Truss support—points $A_1$, $A_2$ | $x'_A$; $y'_A$ | (m) | 0;0 |
| Truss restraint—points $B_1$,$B_2$ | $x'_B$; $y'_B$ | (m) | 0.683; − 0.806 |
| Location of the boom load—point $G$ | $x'_G$; $y'_G$ | (m) | 8.368; − 0.227 |
| Total mass | $m_B$ | (kg) | 922.61 |
| Number of nodes | $n$ | – | 38 |
| Number of members | $m$ | – | 80 |

**Table 2** Comparison of deflections $U$ of the jib loaded with vertical force $F_y$—case P1

| $F_y$ (kN) | $U(m)$ | | $\Delta U_{F_y}$ (m) | $\delta U_{F_y}$ (%) |
|---|---|---|---|---|
| | Autodesk robot | Model | | |
| 10 | 0.009191 | 0.009223 | − 0.000032 | − 0.33 |
| 15 | 0.013786 | 0.013834 | − 0.000048 | − 0.34 |
| 20 | 0.018383 | 0.018445 | − 0.000062 | − 0.34 |
| 25 | 0.022979 | 0.023056 | − 0.000077 | − 0.35 |
| 30 | 0.027575 | 0.027667 | − 0.000092 | − 0.35 |

**Table 3** Comparison of deflections $U$ of the jib loaded with horizontal force $F_z$—case P2

| $F_z$ (kN) | $U(m)$ | | $\Delta U_{F_z}$ (m) | $\delta U_{F_z}$ (%) |
|---|---|---|---|---|
| | Autodesk robot | Model | | |
| 10 | 0.025374 | 0.025445 | − 0.000071 | − 0.28 |
| 15 | 0.038052 | 0.038188 | − 0.000136 | − 0.36 |
| 20 | 0.050726 | 0.050945 | − 0.000219 | − 0.43 |
| 25 | 0.063395 | 0.063719 | − 0.000324 | − 0.51 |
| 30 | 0.076057 | 0.076509 | − 0.000451 | − 0.59 |

**Table 4** Comparison of jib deflection $U$ with respect to inclination angle $\alpha$ of the boom—case P3

| $\alpha$ (deg) | $U(m)$ | | $\Delta U_\alpha$ (m) | $\delta U_\alpha$ (%) |
|---|---|---|---|---|
| | Autodesk robot | Model | | |
| 0 | 0.031389 | 0.031398 | − 0.000009 | − 0.03 |
| 10 | 0.031232 | 0.031336 | − 0.000104 | − 0.33 |
| 20 | 0.030765 | 0.030920 | − 0.000155 | − 0.50 |
| 30 | 0.030033 | 0.030213 | − 0.000180 | − 0.60 |
| 40 | 0.029111 | 0.029308 | − 0.000198 | − 0.68 |
| 50 | 0.028100 | 0.028317 | − 0.000217 | − 0.77 |
| 60 | 0.027123 | 0.027352 | − 0.000229 | − 0.85 |
| 70 | 0.026307 | 0.026524 | − 0.000217 | − 0.83 |
| 80 | 0.025774 | 0.025926 | − 0.000151 | − 0.59 |

**Table 5** Comparison of the natural frequencies of the truss

| $\omega_i$ (Hz) | Autodesk robot | Model | $\Delta\omega_i$ (Hz) | $\delta\omega_i$ (%) |
|---|---|---|---|---|
| $\omega_1$ | 7.73 | 7.80 | − 0.07 | − 0.91 |
| $\omega_2$ | 12.90 | 13.01 | − 0.11 | − 0.85 |
| $\omega_3$ | 28.51 | 28.72 | − 0.21 | − 0.73 |
| $\omega_4$ | 32.42 | 32.56 | − 0.14 | − 0.43 |
| $\omega_5$ | 47.10 | 47.26 | − 0.16 | − 0.34 |

**Table 6** Parameters of the actuator

| Parameter | Symbol | Unit | Value |
|---|---|---|---|
| Outer diameter of the cylinder | $D_{C\text{out}}$ | (m) | 0.165 |
| Inner diameter of the cylinder | $D_{C\text{in}}$ | (m) | 0.14 |
| Minimum length of the actuator | $L_{\min}$ | (m) | 0.36 |
| Extension of the actuator | $L_{\text{str}}$ | (m) | 1.03 |
| Minimum amount of oil in the cylinder | $L_{\text{so}}$ | (m) | 0.10 |

**Table 7** Parameters of the winch and rope system

| Parameter | Symbol | Unit | Value |
|---|---|---|---|
| Winch drive | | | |
| Outer diameter of the drum | $D_{D\text{out}}$ | (m) | 0.287 |
| Inner diameter of the drum | $D_{D\text{in}}$ | (m) | 0.2 |
| Drum length | $L_D$ | (m) | 0.31 |
| Winch mass | $m_W$ | (kg) | 300 |
| Rope system | | | |
| Diameter of the rope | $D_R$ | (m) | 0.013 |
| Density of the rope material | $\rho$ | (kg/m$^3$) | 6500 |
| Modulus of elasticity | $E_L$ | (GPa) | 120 |
| Ratio of the rope system | $i_L$ | (–) | 1 |

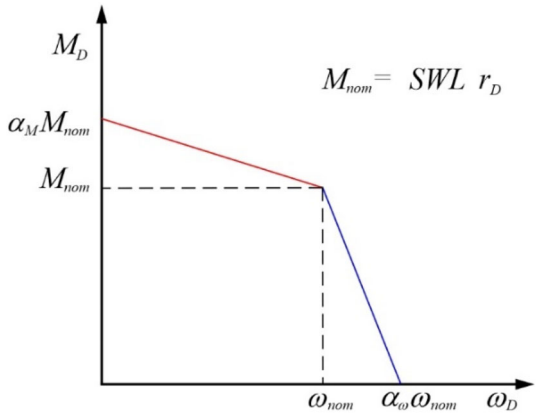


**Fig. 11** Driving torque $M_D$ of the winch, $SWL$ is the safe working load defined as SWL $= m_L g / i_L$, $m_L$ is the load mass, and $i_L$ is the ratio of the rope system from the end of the boom to the load

Further, we present the results of modelling the dynamics of the service crane during the realisation of typical work, taking into account actual operating conditions (i.e., sea waves). These results concern the following tasks:

T1—lifting the load hooked on the rope at a speed changing from zero to nominal speed $v_{\text{nom}}$ for the boom inclination angle $\alpha = 50°$ (torque characteristics $M_D$ is presented in Fig. 11).

T2—picking up cargo from the deck of a stationary supply vessel. Driving torque $M_D$ and angle $\alpha$ are as in T1; the initial tension of the rope equals 0.

T3—lifting the load from the deck of a stationary supply vessel for various values of inclination angle $\alpha$ of the jib to the horizontal. Driving torque $M_D$ is assumed as in T1.

T4—maintaining a constant operating tension in the rope when the load rests on the deck of the supply vessel. Regular sea waves are considered, and the boom inclination angle is $\alpha = 30°$.

T5—column rotation for various boom inclination angles.

T6—column rotation for different load masses attached to the rope.

In tasks T1,…,T6, the value of overload coefficient $\psi$ in the rope system is analysed. The following formula is used to determine the value of coefficient $\psi$:

$$\psi = S/SWL, \tag{40}$$

where $S$ is the force in the rope.

For the numerical simulations, it is assumed that $i_L = 1$ (Table 7).

In task T1, at time $t = 0$, the rope is loaded with mass $m_L$ and $S = \text{SWL}$. In tasks T2 and T3, the force in the rope at the beginning equals zero (mass $m_L$ remains on the deck of the supply vessel). Torque characteristics $M_D$ (Fig. 11) mean that, with the assumption of $\alpha_M = 1.3$ and $\alpha_\omega = 1.5$, the load leaves the supply vessel's deck after only about 0.1 s. In the case of T4, and the torque acting on the drum winch $M_D = 1.3 M_{\text{nom}}$ is constant. Therefore, the torque reflects AOPS (Automatic Overload Protection System), in which the activation and deactivation values are assumed to be equal to 1.3.

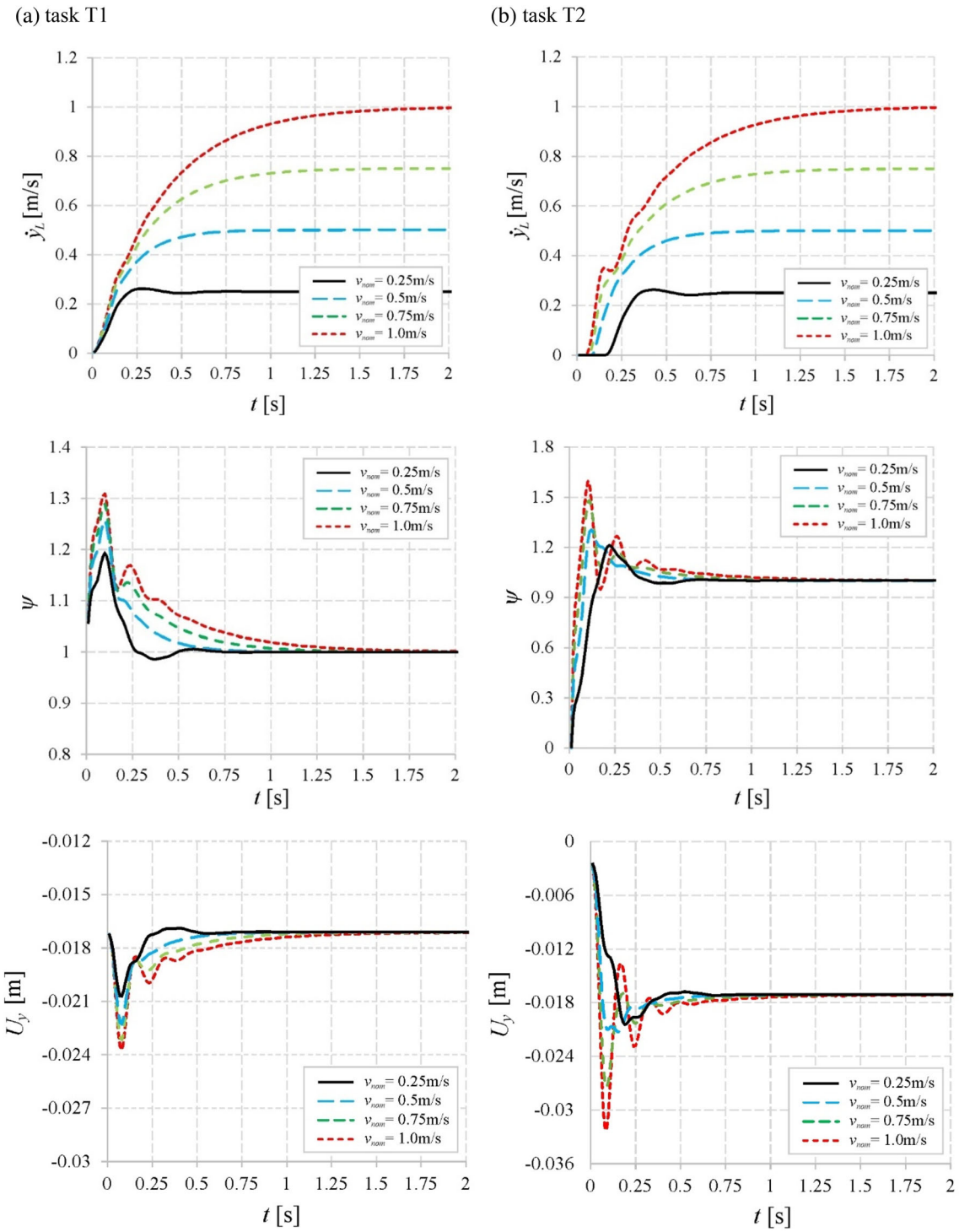


**Fig. 12** Lifting of the load **a** in the air—task T1, **b** from the deck of a supply vessel—task 2, courses of: vertical speed of the load $\dot{y}_L$, overload coefficient in the rope $\psi$, vertical deflection of the boom $U_y$

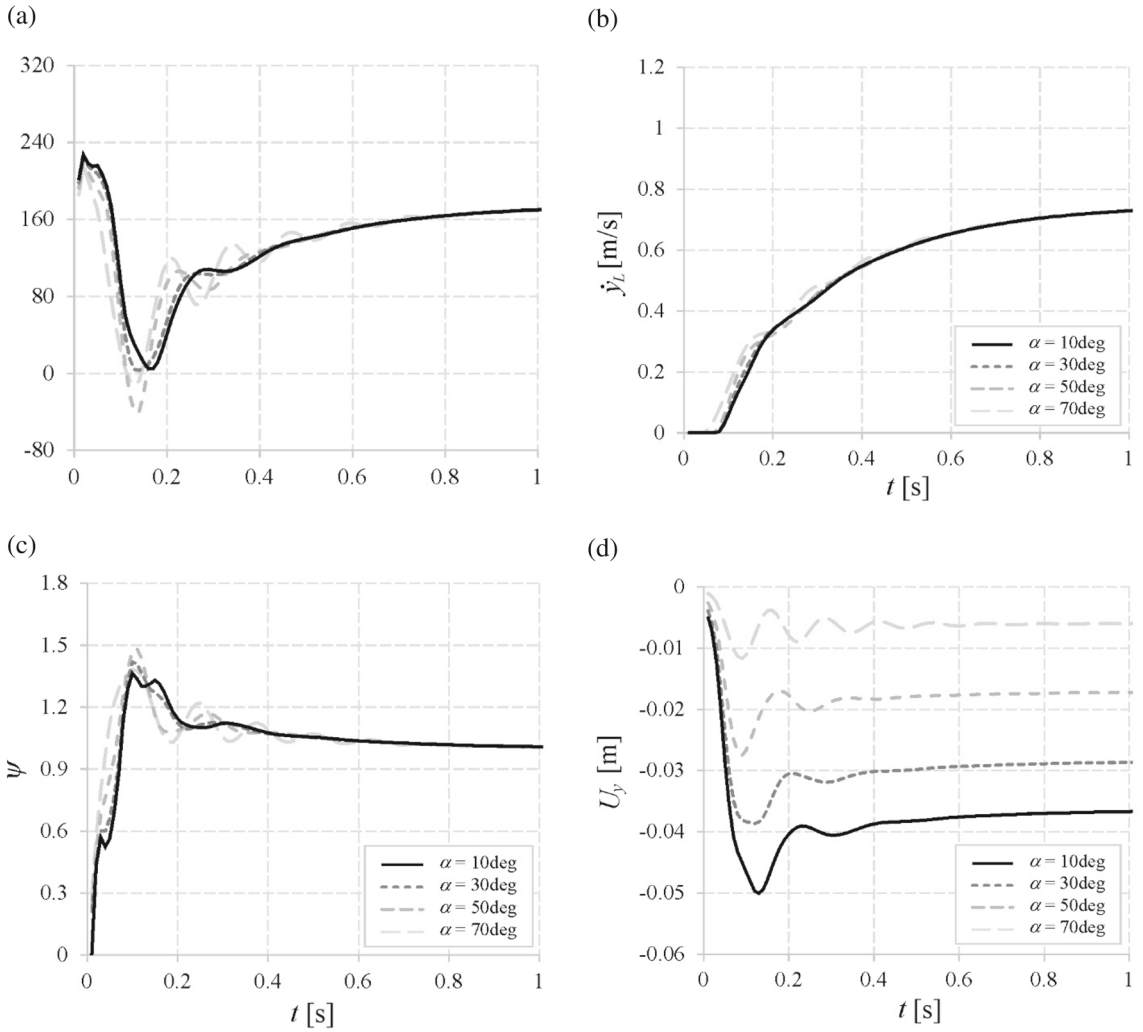


**Fig. 13** Lifting the load from the deck of a supply vessel for various boom inclination angles $\alpha$—task T3, courses: **a** rotational speed of the winch drum $\dot{\varphi}_D$, **b** vertical speed of the load $\dot{y}_L$, **c** overload coefficient in the rope $\psi$, and **d** vertical deflection of the boom $U_y$

Graphs concerning lifting of the cargo in the air—task T1—are presented in Fig. 12a. They show a clear influence of the nominal speed $v_{\text{nom}}$ of load lifting on the value of the overload $\psi$ in the rope and vertical deflection $U_y$ of the boom. The value of the overload coefficient for nominal speed $v_{\text{nom}} > 0.75\,\text{m/s}$ is exceeded by more than 30% compared to the situation when the load attached to the rope hangs freely. Vertical deflection $U_y$ of the jib increases with the increase of the nominal speed of lifting the load. This is especially noticeable in the initial time of simulations ($t < 0.25$). A similar situation is observed in task T2 (Fig. 12b), with the difference that the courses of $\psi$ and $U_y$ show greater overload in the rope and deflections of the boom. In this case, the vibrations are initiated by the cargo leaving the supply vessel.

In task T3, the influence of the boom inclination angle $\alpha$ on the load of the rope system and on the crane structure is analysed while lifting a load with a given mass. Simulations of the lifting are carried out for the load with mass $m_L = 2000$ kg, having assumed that the load reaches nominal lifting speed $v_{\text{nom}} = 0.75$ m/s. The results of simulations are presented in Fig. 13. Increasing the boom inclination angle $\alpha$, while lifting the load with the same mass, clearly reduces vertical deflections of the boom; see courses $U_y$ in Fig. 13d. Despite the significant differences in courses of deflections, the maximum value of the overload coefficient $\psi$ in the rope for individual cases is within the limits of $\langle 1.36;\ 1.48\rangle$. The difference between the extreme overload values is approx. 7%.

In turn, in task T4, the influence of the amplitude of waves acting on a supply vessel on the overload of the rope system is investigated when the load rests on a deck of the vessel. Regular waves with amplitudes $A_i \epsilon \langle 1,\ 3\rangle$m are examined. At the same time, it is assumed that the platform on which the crane is placed is stationary. Initial position of the load (at $t = 0$ s) for boom inclination angle $\alpha = 30°$ is $x_L = x_G = 7.36$ m, $y_L = -10$ m, and $z_L = 0$.

C1) $H_{S,x} = H_{S,z} = 0, H_{S,y} \epsilon \langle 2,6 \rangle$

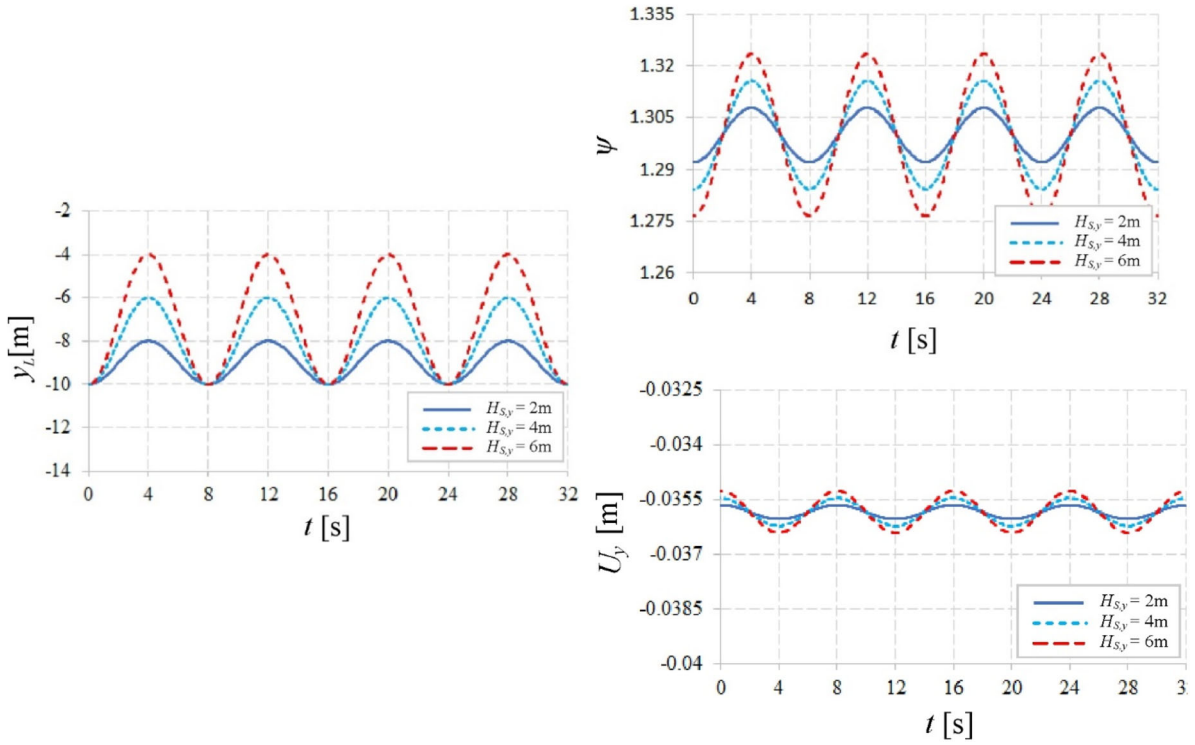


C2) $H_{S,x} \epsilon \langle 2,6 \rangle, H_{S,y} = 0, H_{S,z} \epsilon \langle 1,3 \rangle$

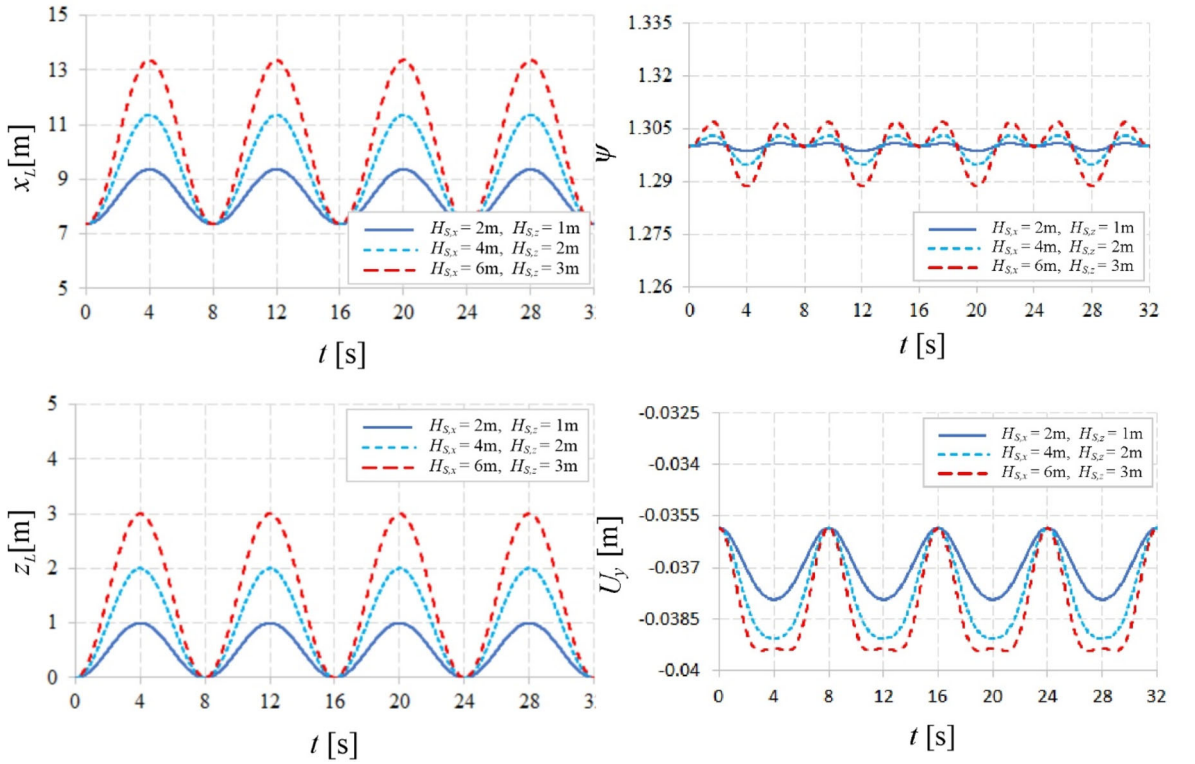


**Fig. 14** Maintaining the operating tension in the rope—task T4, cases C1 and C2, courses of $h_i^L$, overload coefficient $\psi$ and vertical deflection of the boom $U_y$

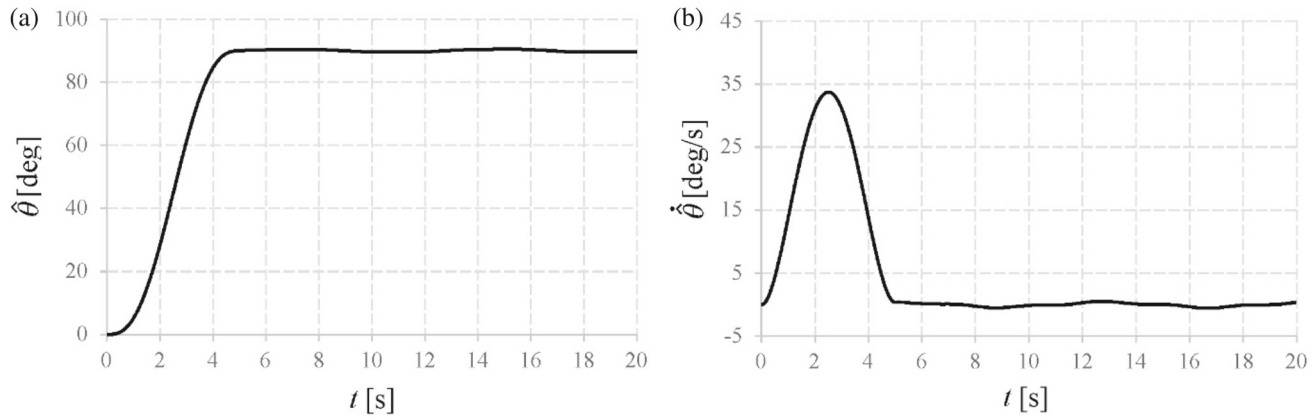


**Fig. 15** Rotation angle $\widehat{\theta}_P$ and angular velocity $\dot{\widehat{\theta}}_P$ of the column in tasks T5 and T6

Courses of the regular wave are described by the following relation:

$$h_i^L(t) = A_i\left(1 - \cos\omega_{P,i}t\right), \text{ for } i = x,\ y,\ z, \tag{41}$$

where $A_i = \frac{1}{2}H_{s,i}$ is the amplitude of the wave in direction $i$, $H_{s,i}$ is the wave height, $T_{P,i}$ is the wave period, $\omega_{P,i} = \frac{2\pi}{T_{P,i}}$ is the wave frequency, and $t$ is time.

It is assumed that the load is placed under point $G$ of the boom (Fig. 10), 10m below plane $xz$ (Fig. 1), and thus

$$\begin{aligned} x_L &= x_G^0 + h_x^l \\ y_L &= -10 + h_y^l, \\ z_L &= z_G^0 + h_z^l \end{aligned} \tag{42}$$

where $x_G^0$, $z_G^0$ are coordinates of point $G$ for $t = 0$.

The height and period of the regular wave are assumed as follows: $H_{S,x} = H_{S,z} = 0$, $H_{S,y}\epsilon\langle 2,\ 6\rangle$m (case C1) or $H_{S,y} = 0$, $H_{S,x} = H_{S,z}\epsilon\langle 2,\ 6\rangle$m (case C2) and $T_{P,i} = 8$s.

The results of simulations of task T4, and the courses of the position of load $x_L$, $y_L$, $z_L$, of overload coefficient $\psi$, and of vertical deflection of the boom $U_y$, with respect to the assumed combination of wave parameters $H_{S,i}$, are presented in Fig. 14.

In both analysed cases, a different range of variability of overload coefficient $\psi$ is obtained. In the case of C1, when the supply vessel is only moving vertically, coefficient $\psi$ is between $\langle 1.276$ and $1.325\rangle$. Much smaller values of the overload in the rope occur when the vessel's motion is considered in the horizontal plane; then, $\psi\epsilon\langle 1.289;\ 1.307\rangle$. However, the situation is different with vertical deflection $U_y$ of the boom. As a result of the horizontal movement of the supply vessel in plane $yz$, much greater vertical deflections of the boom are observed than when the load resting on the deck moves only vertically.

The next two tasks (T5 and T6) are concerned with simulation of the rotation of the crane column with a load attached at the end of the rope. The influence of boom inclination angle $\alpha$ and load mass $m_L$ on the deflection of the crane structure and overload of the rope system are analysed. The course of the kinematic input, rotation angle of the crane column $\theta_P$, and its velocity are presented in Fig. 15.

Simulation results obtained in our own programme for various values of parameters $\alpha$ and $m_L$ are shown in Fig. 16. In the simulations, the boom inclination angle is constant and is $\alpha = 50^{\circ}$.

Having analysed the simulation results concerning the rotation of the crane column (tasks T5 and T6), a significant influence of the inclination angle of the boom on overload coefficient $\psi$ can be seen. In task T5, the maximum value of the overload coefficient for inclination angle $\alpha = 70°$ is 1.05, and for angle $\alpha = 10°$, the maximal value of coefficient $\psi$ is 1.32. However, in task T6, the maximum value of $\psi$ is close to 1.15 in all courses. This is due to the fact that during rotation of the crane column with a load attached to the end of the rope, almost identical courses of coefficient $\psi$ are obtained.

As could be expected, both the reduction of the boom inclination angle and the increase of the load mass cause greater changes in the vertical and horizontal deflections of the crane. To support this conclusion, Table 8 summarises the maximum values of the amplitudes of vertical and horizontal deflection of the boom in both tasks concerning rotation of the crane column.

## 6 Final remarks

The paper presents a spatial model of the dynamics of a lattice jib crane. The Rigid Finite Element Method is used for discretisation and the translational and rotational displacements in the truss nodes are assumed as generalised

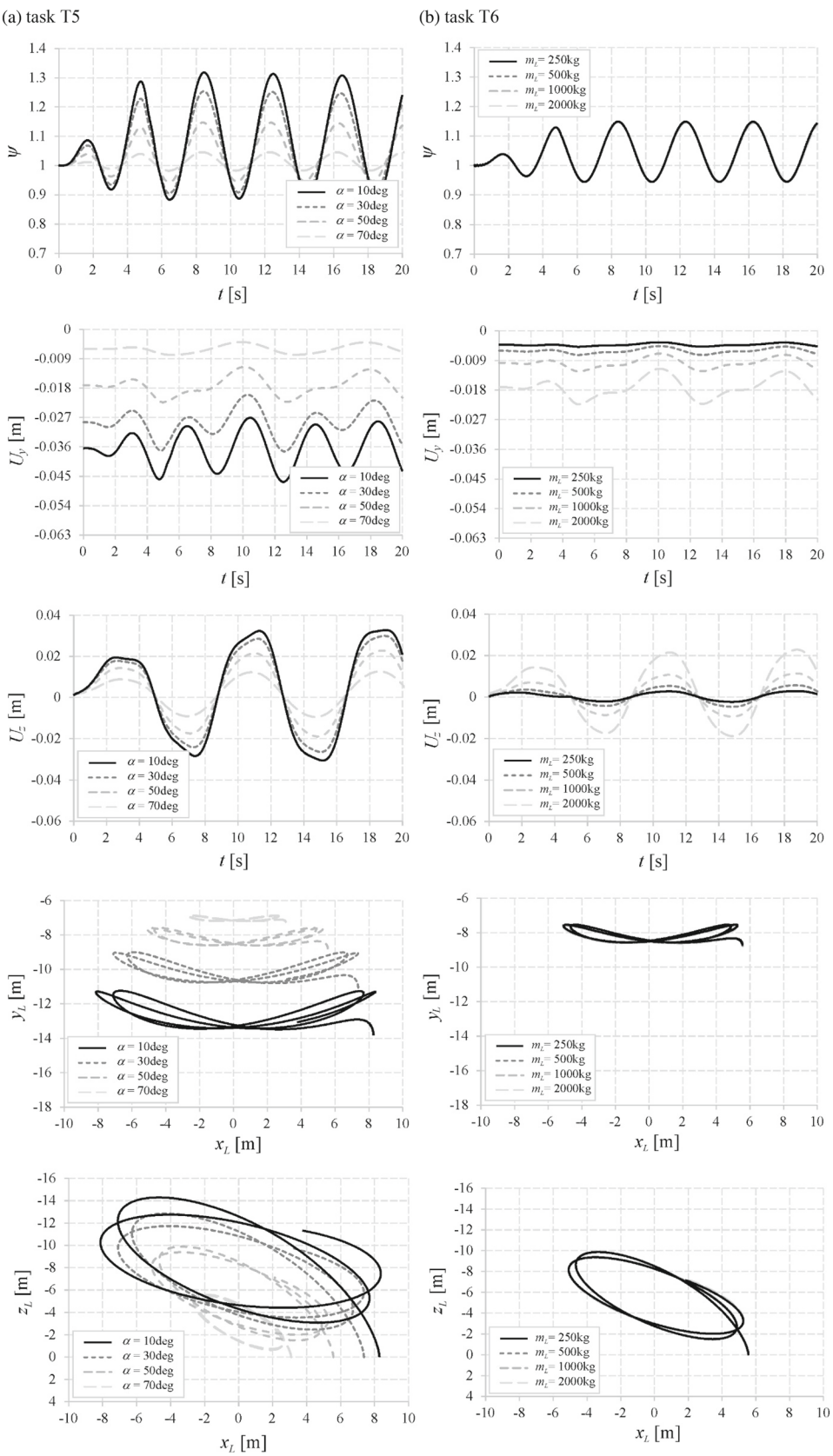


**Fig. 16** Rotation of the crane column with a load attached at the end of the rope—tasks T5 and T6, courses of: overload coefficient $\psi$, components $U_y$, $U_z$ of the deflection of the boom, trajectories of the load: projections on $xy$ and $xz$ planes

**Table 8** Maximum amplitudes of vertical $A_{Uy}$ and horizontal $A_{Uz}$ deflections of the crane in tasks T5 and T6

| Task T5 | | | Task T6 | | |
|---|---|---|---|---|---|
| $\alpha$ (deg) | $A_{Uy}$ (m) | $A_{Uz}$ (m) | $m_L$ (kg) | $A_{Uy}$ (m) | $A_{Uz}$ (m) |
| 10 | 0.0103 | 0.0317 | 250 | 0.0007 | 0.0026 |
| 30 | 0.0089 | 0.0285 | 500 | 0.0014 | 0.0053 |
| 50 | 0.0056 | 0.0212 | 1000 | 0.0028 | 0.0106 |
| 70 | 0.0021 | 0.0111 | 2000 | 0.0056 | 0.0212 |

coordinates. The nodes of the truss also contain the mass features of the truss members. On the other hand, flexible features are reflected by massless spring–damping elements located in the middle of the truss members. The advantage of the method proposed for discretisation of the lattice boom is simplicity and ease of physical interpretation. A computer programme has been developed on the basis of the mathematical model elaborated. The results obtained in the authors' own programme have been compared with those obtained using a commercial software package. Both for static deflections and frequencies of free vibrations, the relative errors do not exceed 1%. Moreover, with the use of the model, simulations of the crane dynamics during transport operations have been carried out taking into account sea conditions. The problems considered included: lifting the cargo in the air and from the deck of a supply vessel, maintaining constant tension in the rope system, and rotation of the crane column. The simulations performed enable deformation of the crane structure and overload in the rope system to be analysed before the crane is manufactured and used in real conditions. This is the first model of crane dynamics for truss jibs to use the rigid finite element method for discretisation of the truss members.

## Declarations

**Conflict of interest** The authors have no relevant financial or non-financial interests to disclose.



## References

Abdel-Rahman EM, Nayfeh AH, Masoud ZN (2003) Dynamics and control of cranes: a review. J Vib Control 9(7):863–908. https://doi.org/10.1177/1077546303009007007

Adamiec-Wójcik I, Drąg Ł, Wojciech S, Metelski M (2018) Application of the rigid finite element method to static analysis of lattice-boom cranes. Int J Appl Mech Eng 23(3):803–811. https://doi.org/10.2478/ijame-2018-0044

Adamiec-Wójcik I, Drąg Ł, Metelski M, Nadratowski K, Wojciech S (2019) A 3D model for static and dynamic analysis of an offshore knuckle boom crane. Appl Math Model 66:256–274. https://doi.org/10.1016/j.apm.2018.09.006

Arena A, Casalotti A, Lacarbonara W, Cartmell MP (2015) Dynamics of container cranes: three-dimensional modeling, full-scale experiments, and identification. Int J Mech Sci 93:8–21. https://doi.org/10.1016/j.ijmecsci.2014.11.024

Bak MK, Hansen MR (2013) Analysis of offshore knuckle boom crane-part one: modeling and parameter identication. Model Identif Control 34(4):157–174. https://doi.org/10.4173/mic.2013.4.1

Cao Y, Li T (2020) Review of antiswing control of shipboard cranes. IEEE/CAA J Autom Sin 7(2):346–354. https://doi.org/10.1109/JAS.2020.1003024

Cha JH, Il RM, Lee KY (2010) Dynamic response simulation of a heavy cargo suspended by a floating crane based on multibody system dynamics. Ocean Eng 37(14–15):1273–1291. https://doi.org/10.1016/j.oceaneng.2010.06.008

Chu Y, Æsøy V, Ehlers S, Zhang H (2015) Integrated multi-domain system modelling and simulation for offshore crane operations. Ship Technol Res 62(1):36–46. https://doi.org/10.1179/0937725515Z.0000000004

Chu Y, Hatledal LI, Zhang H, Aesøy V, Ehlers S (2018) Virtual prototyping for maritime crane design and operations. J Mar Sci Technol 23:754–766. https://doi.org/10.1007/s00773-017-0509-z

Cibicik A, Egeland O (2019) Dynamic modelling and force analysis of a knuckle boom crane using screw theory. Mech Mach Theory 133:179–194. https://doi.org/10.1016/j.mechmachtheory.2018.10.019

Craig JJ (1989) Introduction to robotics: mechanics and control, 2nd edn. Pearson, London

Doçi I, Hamidi B, Lajqi S (2016) Dynamic analysis and control of jib crane in case of jib luffing motion using modelling and simulations. IFAC-PapersOnLine 49(29):163–168. https://doi.org/10.1016/j.ifacol.2016.11.094

Hong KS, Ngo QH (2012) Dynamics of the container crane on a mobile harbor. Ocean Eng 53:16–24. https://doi.org/10.1016/j.oceaneng.2012.06.013

Krukowski J, Maczyński A (2013) Application of the rigid finite element method for modelling an offshore pedestal crane. Arch Mech Eng 60(3):451–471.https://doi.org/10.2478/meceng-2013-0028

Kruszewski J, Gawroński W, Wittbrodt E, Najbar F, Grabowski S (1975) Rigid finite element method (Metoda sztywnych elementów skończonych), 1st edn. Arkady, Warszawa

Maczyński A, Wojciech S (2011) Stabilization of load's position in offshore cranes. J Offshore Mech Arct Eng 134(2):021101. https://doi.org/10.1115/1.4004956

Maourane H, Szabó T (2020) Linear and nonlinear dynamical analysis of a crane model. Pollack Period 15(2):82–93. https://doi.org/10.1556/606.2020.15.2.8

Nowak P, Nowak A, Metelski M (2017) Modelling of vibration and large deflections of lattice-boom structures of cranes by means of rigid finite element method. In: Awrajcewicz J, Kaźmierczak M, Mrozowski J, Olejnik P (eds) Mathematical and numerical aspects of dynamical system analysis. Lodz University of Technology, Łódź, pp 425–436

Osiński M, Wojciech S (1998) Application of nonlinear optimisation methods to input shaping of the hoist drive of an offshore crane. Nonlinear Dyn 17:369–386. https://doi.org/10.1023/A:1008333417693

Osiński M, Maczyński A, Wojciech S (2004) The influence of ship's motion in regular wave on dynamics of an offshore crane. Arch Mech Eng 51(2):131–163

Raja Ismail RMT, That ND, Ha QP (2015) Modelling and robust trajectory following for offshore container crane systems. Autom Constr 59:179–187. https://doi.org/10.1016/j.autcon.2015.05.003

Ramli L, Mohamed Z, Abdullahi AM, Jaafar HI, Lazim IM (2017) Control strategies for crane systems: a comprehensive review. Mech Syst Signal Process 95:1–23

Ren H, Wang X, Hu Y, Li C (2008) Dynamic response analysis of a moored crane-ship with a flexible boom. J Zhejiang Univ A 9:26–31. https://doi.org/10.1631/jzus.A071308

Rong B, Rui X, Lu K, Tao L, Wang G, Yang F (2019) Dynamics analysis and wave compensation control design of ship's seaborne supply by discrete time transfer matrix method of multibody system. Mech Syst Signal Process 128:50–68. https://doi.org/10.1016/j.ymssp.2019.03.006

Trąbka A (2016) Influence of flexibilities of cranes structural components on load trajectory. J Mech Sci Technol 30:1–14. https://doi.org/10.1007/s12206-015-1201-z

Urbaś A, Szczotka M, Maczyński A (2010) Analysis of movement of the BOP crane under sea weaving conditions. J Theor Appl Mech 48(3):677–701

Wittbrodt E, Adamiec-Wójcik I, Wojciech S (2006) Dynamics of flexible multibody systems rigid finite element method, 1st edn. Springer, Berlin

Wittbrodt E, Szczotka M, Maczyński A, Wojciech S (2013) Rigid finite element method in analysis of dynamics of offshore structures, 1st edn. Springer, Berlin